Preparation of Si-Zr-C Composite Coating on C/C Composite Material by Infiltration Method and Study on Anti-Ablation Performance

Shuaipeng Li, Xueni Guo

Henan Mechanical & Electrical Vocational College, Zhengzhou Henan 450000, China

Abstract: This study investigates the effect of the Si/Zr mass ratio on the morphology, phase composition, and anti-ablation performance of Si-Zr-C composite coatings on C/C composite materials by controlling the Si/Zr mass ratio in the infiltration material. With an increase in the Si/Zr mass ratio in the infiltration material, the coating becomes smoother, and there are changes in the phase composition of the coating. Through ablation testing, it was observed that the anti-ablation performance of the coating initially increases and then decreases with an increase in the Si/Zr mass ratio. The best anti-ablation performance is exhibited when the Si/Zr mass ratio is 6:4, with a mass ablation rate of -3.083×10^{-5}/ $g\cdot s^{-1}$ after 120s of ablation. The presence of fewer cracks and grain boundaries on the coating surface results in higher coating strength. Additionally, the reaction products ZrO_2 and $ZrSiO_4$ enhance the high-temperature stability of SiO_2. Moreover, they themselves possess good anti-ablation performance and a lower oxygen diffusion rate, thereby improving the anti-ablation performance of the coating.

Keywords: Si/Zr mass ratio; C/C composite materials; Anti-ablation performance; Infiltration method

1 Preparation of Si-Zr-C Composite Coating

Different Si-Zr-C composite coatings with varied structural morphologies were obtained by controlling the Si/Zr mass ratio in the infiltration material. The influence of the Si/Zr mass ratio in the infiltration material on the morphology and anti-ablation performance of Si-Zr-C composite coatings was studied. To facilitate infiltration into the matrix during the process, vacuum atmosphere was employed. Additionally, to minimize the damage to C fibers caused by high-temperature reactions during the infiltration process, the infiltration temperature was set at 1750℃. The specific process parameters are as follows:

Table 1 Si-Zr-C multilayer coating processing parameters

No.	Si/Zr mass ratio in the embedding material	Atmospheres	Temp	Time
1	4:6	vacuums	1750℃	2h
2	5:5	vacuums	1750℃	2h
3	6:4	vacuums	1750℃	2h
4	7:3	vacuums	1750℃	2h

2 Influence of Si/Zr Mass Ratio in Infiltration Material on Surface Morphology of Composite Coatings

Figures 1a, b, c, and d respectively depict the surface morphology of samples 1, 2, 3, and 4 of composite coatings. From the figures, it can be observed that the surface of sample 1 exhibits complete crystallization, but there are small pores between grains, indicating low coating density. Additionally, cracks are present on the surface, possibly due to thermal stress generated during the cooling process as a result of mismatched coefficients of thermal expansion between the coating and the substrate.

The surface of sample 2 shows significant changes compared to sample 1. It is extremely rough, yet denser with no apparent pores. The surface consists of a mixture of two types of grains, but further observation is required to confirm this. The grains are coarse, with clearly visible protruding grains and distinct grain boundaries. Most cracks are found at grain boundaries, indicating that grain boundaries provide some relief from thermal stress. However, they also serve as active sites for ablation, and the presence of cracks makes the grains susceptible to detachment under thermal stress and gas shear forces, leading to substrate ablation.

Sample 3 exhibits considerable differences in surface morphology compared to sample 2 but still consists of a mixture of two types of grains dispersed throughout

the surface. The coating appears denser with intact crystallization, coarse grains, and visible grain boundaries. However, compared to sample 2, the surface of sample 3 is smoother with fewer cracks, indicating good physical compatibility with the substrate and minimal difference in coefficients of thermal expansion between the coating and the substrate.

Most of the surface of sample 4 is covered with grains of approximately 20μm in size, with pores present between grains, resulting in poor coating density. Some areas above the grains are covered with a glassy substance, possibly indicating a different phase from the grains, which requires further analysis. Cracks are also present on the surface. The pores and cracks on the coating surface can serve as pathways for direct ablation of the substrate by gas flow during the initial stages of ablation, adversely affecting the anti-ablation performance of the coating.

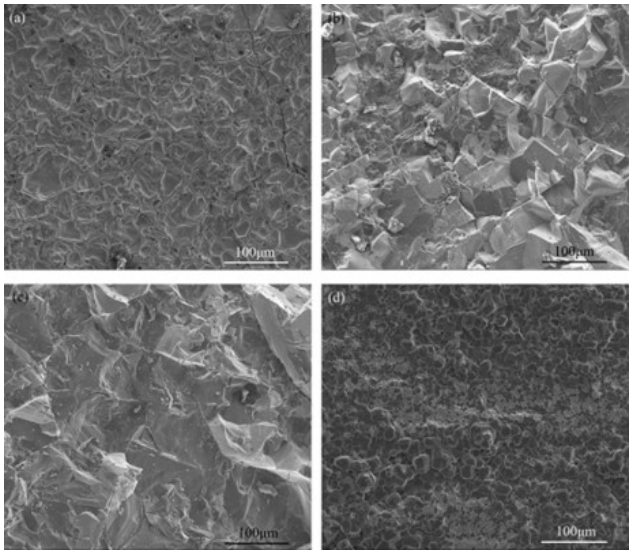

Figure 1 Surface micrographs (a,b,c,d)of multilayer coating in sample 1,2,3,4

3 Influence of Si/Zr Mass Ratio in Infiltration Material on Surface Phase Composition of Composite Coatings

Figures 2(a) and (b) respectively depict the surface and cross-sectional backscattered electron micrographs of sample 1. From Figure 2(a), it can be observed that the surface coating of sample 1 is composed of a single white phase. Spectral analysis of the coating surface in Figure 4 and XRD analysis in Figure 3 confirm that the white phase is ZrC. Figure 2(b) shows the cross-sectional morphology of the coating. The coating consists of two parts: a gray-white mixed coating that is well bonded to the substrate and a white ZrC coating covering the gray-white mixed coating. Analysis reveals that the gray-white coating is composed of SiC. During the infiltration process, Si in the infiltration material reaches its melting point and melts first. Due to the good wettability of Si with the carbon matrix, molten Si drives some Zr to flow into the interior of the substrate through surface pores, reacting with the carbon matrix to form a SiC-ZrC mixed coating. As the infiltration progresses, a large amount of Si infiltrates into the interior of the substrate, resulting in the formation of a thin SiC-ZrC coating only on the surface of the substrate. With the decrease in Si content in the infiltration material, Zr in the infiltration material reacts with the carbon matrix through diffusion to generate an outer layer of ZrC. From the cross-sectional view of the coating, it can be seen that the SiC-ZrC mixed coating infiltrates into the interior of the substrate and fills the gaps between the fibers, tightly bonding with the substrate. The coating and the substrate are wedged together, enhancing the physical strength of the bond. The inner and outer layers of the coating are closely bonded, and no obvious interface is observed. However, there is a significant difference in the coefficients of expansion between ZrC (7.3×10^{-6}/K) and SiC (4.3×10^{-6}/K). When the coating is exposed to ablation environments, this mismatch in thermal expansion between the inner and outer layers of the coating may lead to thermal stress, causing cracks or even delamination on the surface of the coating.

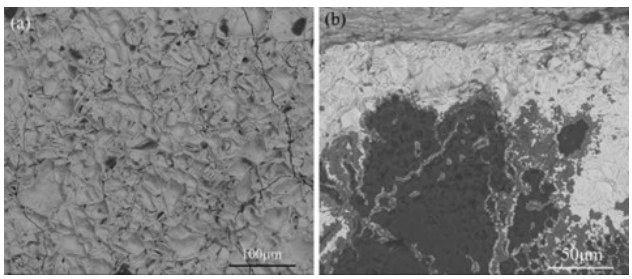

Figure 2 Surface BSE image(a) and cross-section(b) BSE image of sample 1

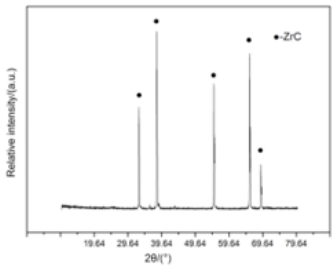

Figure 3 XRD patterns of sample 1

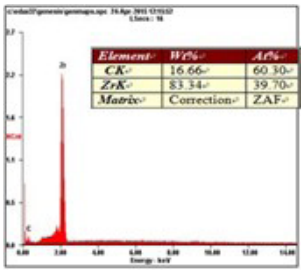

Figure 4 EDS image of sample 1

Figure 5(a) and (b) respectively show the surface and cross-sectional backscattered electron micrographs of sample 2. From Figure 5(a), it can be observed that the coating surface is rough and composed of white and gray phases. The interface between the two phases is apparent, and cracks are observed at some interfaces. Observing Figure 5(b), the cross-sectional view of the coating reveals that the gray phase coating is tightly bonded to the substrate, with the mixture of gray and white phases penetrating into the interior of the substrate, wedged with the substrate. A layer of mixed gray-white phase composite coating covers the surface of the gray phase coating, with tight bonding between the coatings and no obvious interface detected.

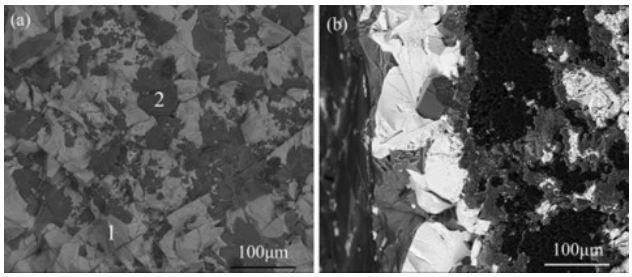

Figure 5 BSE image of surface(a) and cross-section(b) in coated sample 2

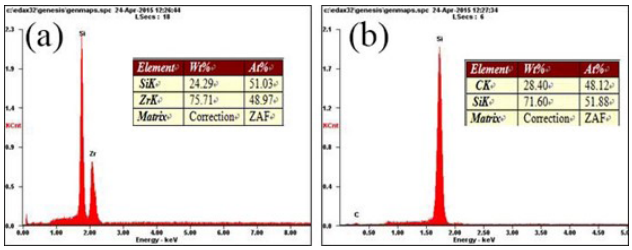

Figure 6 BSE analysis of point 1,2 in coating surface

Figure 6(a) and (b) respectively display the energy spectrum analysis at points 1 (white phase) and 2 (gray phase) on the surface of the coating. By comparing with the XRD analysis spectrum of the coating surface in Figure 7, it can be inferred that the white phase in the coating is ZrSi, while the gray phase is SiC.

During the infiltration process, Si in the infiltration material melts first. Molten Si drives Zr in the powder to infiltrate into the interior of the substrate, reacting to form the coating, establishing both chemical and wedge-shaped physical bonds with the substrate. As the reaction proceeds, a layer of SiC inner layer forms on the substrate surface, isolating the infiltration material from the substrate. The infiltration material mainly reacts with the substrate through diffusion. Molten Si, due to its good flowability, effectively covers the surface of the SiC inner layer. Zr, which remains unmelted at the infiltration temperature, diffuses through the SiC inner layer, where carbon (C) reacts preferentially with molten Si to form SiC. Simultaneously, molten Si reacts with Zr. Since Si reacts first with the substrate, the Si/Zr mass ratio in the infiltration material should be less than 5:5.

Figure 8 depicts the Si-Zr phase diagram. Observing the phase diagram, it can be deduced that under the current Si/Zr mass ratio in the infiltration material, ZrSi is the most likely compound to be formed, consistent with the analysis results.

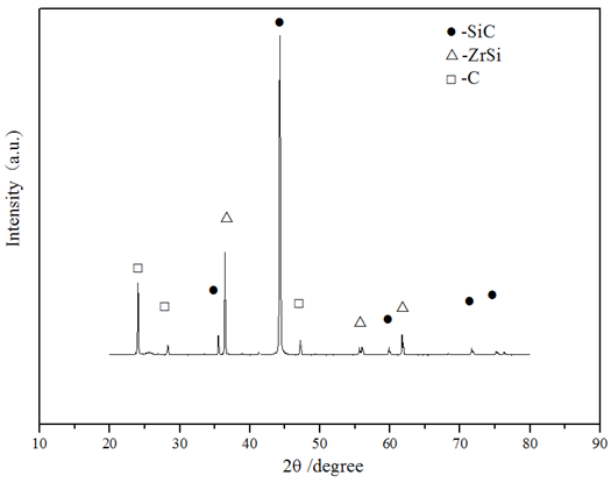

Figure 7 XRD patterns of sample 2

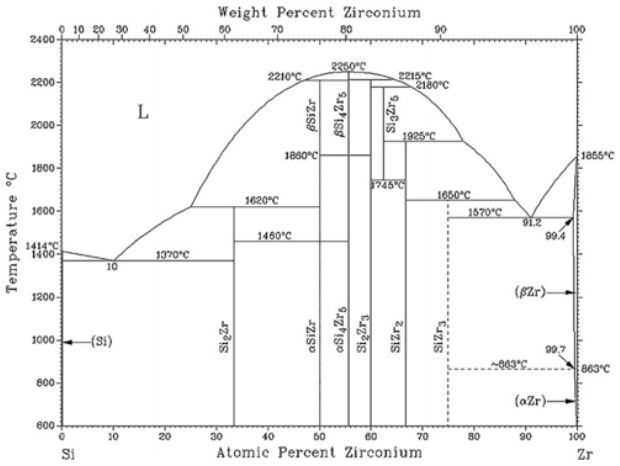

Figure 8 Si-Zr phase diagram

Figure 9(a) and (b) respectively depict the backscattered images of the surface and cross-section of sample 3. From Figure 9(a), it can be observed that the surface of the coating is composed of three phases: dark gray (point 1), gray (point 2), and white (point 3). The white and gray phases exhibit complete crystallization with coarse grains. There is a distinct interface between the white and gray phases. The dark gray phase is less abundant and is distributed between the gray and white phases. The surface of the coating is smoother compared to sample 2, with fewer cracks and a reduced presence of the white phase, leading to a decrease in the interface between the white and gray phases compared to sample 2.

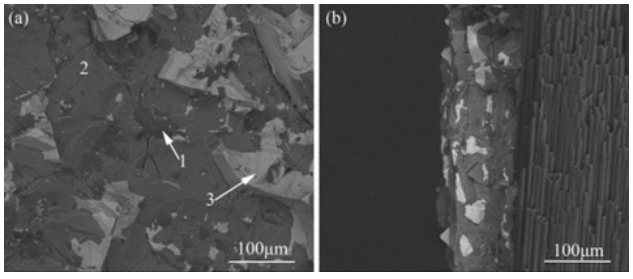

Figure 9 BSE image of surface(a) and cross-section(b) in coated sample 3

Figure 10(a), (b), and (c) correspond to the energy spectrum analysis of points 1, 2, and 3 on the coating surface, respectively, as well as the dark gray, gray, and white phases. Combining with Figure 11, the XRD analysis of the coating surface reveals that the dark gray phase on the surface is Si, the gray phase is SiC, and the white phase is $ZrSi_2$.

Upon observation of Figure 9(b), it is noted that the coating cross-section consists of two layers. The inner layer of the coating is composed of SiC, tightly bonded to the substrate. No distinct interface is observed between the coating and the substrate at the interface. The outer layer of the SiC coating is a SiC-$ZrSi_2$-Si composite coating, which is dense overall, with no visible penetrating cracks or voids.

During the infiltration process, Si melts first and infiltrates into the interior of the substrate while simultaneously covering the substrate surface. Within the substrate, Si reacts with the carbon to form the SiC inner layer. As the reaction progresses, carbon from the substrate continues to diffuse through the SiC inner layer to react with the infiltration material. Since only Si is melted in the infiltration material, molten Si preferentially covers the surface of the SiC coating and reacts with the carbon in the substrate through diffusion, further developing the SiC coating. Meanwhile, as the Si content decreases in the infiltration material and the Si/Zr mass ratio is less than 6:4, Si reacts with Zr to form $ZrSi_2$, consistent with the phase diagram results in Figure 8. As the reaction proceeds, a small amount of molten Si remains in the infiltration material and does not react with the carbon in the substrate or with Zr in the infiltration material, leading to the presence of a small amount of Si in the coating.

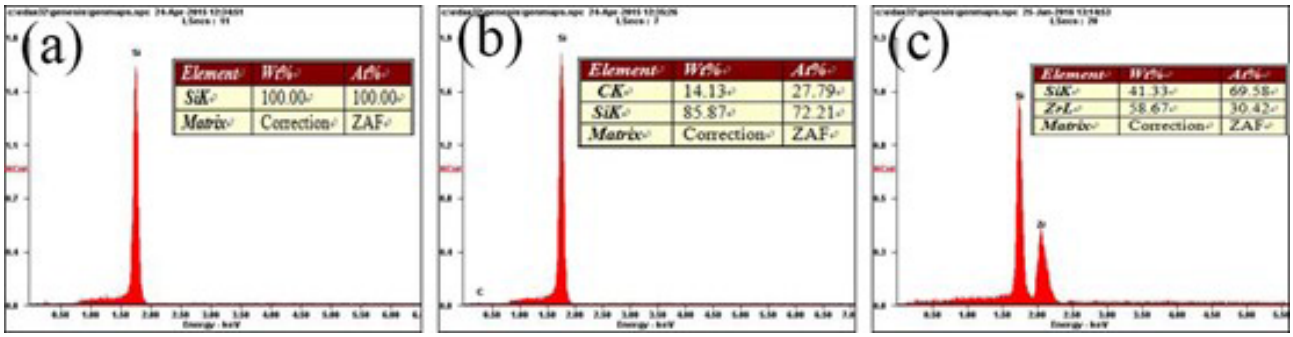

Figure 10 EDS analysis(a,b,c) of point 1,2,3 in coating surface of sample 3

Figure 11 XRD patterns of sample 3

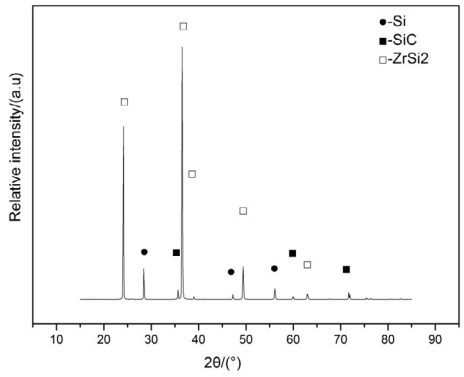

Figure 12(a) and (b) respectively depict the backscattered images of the surface and cross-section of sample 4. Figure13(a) and (b) respectively show the energy spectrum analysis spectra of the gray phase (point 1) and the white phase (point 2) on the surface of sample 4.

From Figure 12(a), it can be observed that the surface of the coating is relatively smooth, composed of white and gray phases. The gray phase dominates most of the coating, while the white phase is distributed within the gray phase. The gray phase on the surface of the coating exhibits complete crystallization, but there are pores between grains. Cracks are present on the surface of the coating, and the white phase appears glassy.

Figure 12 Surface BSE image(a) and cross-section BSE image(b) of coating in sample 4

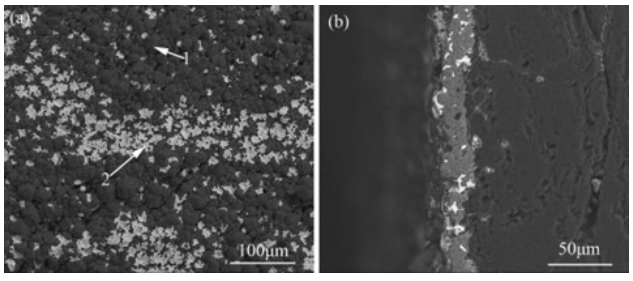

Figure 13 EDS analysis of point1,2(a,b) in surface of sample 4 coating

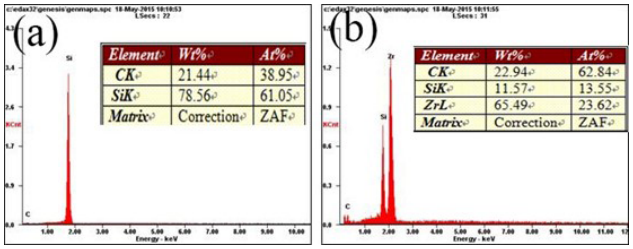

Combining with the XRD analysis spectra of the coating surface in Figure 14, it is evident that the white phase on the surface of the coating is ZrC, while the gray phase is SiC. Observing Figure 12(b), the cross-section of the coating is dense, with no visible penetrating cracks or voids. The coating is composed of SiC and a small amount of ZrC.

During the infiltration process, molten Si first reacts with the carbon in the substrate to form a SiC coating. Simultaneously, it reacts with Zr to form $ZrSi_2$. However, due to the thinness of the formed SiC coating and the low Zr content in the infiltration material, $ZrSi_2$ reacts with the carbon in the substrate through diffusion to form ZrC and SiC. Upon completion of the reaction, most of the coating surface is covered by the SiC coating, with only a small amount of ZrC present.

Figure 14 XRD patterns of sample 4 coating

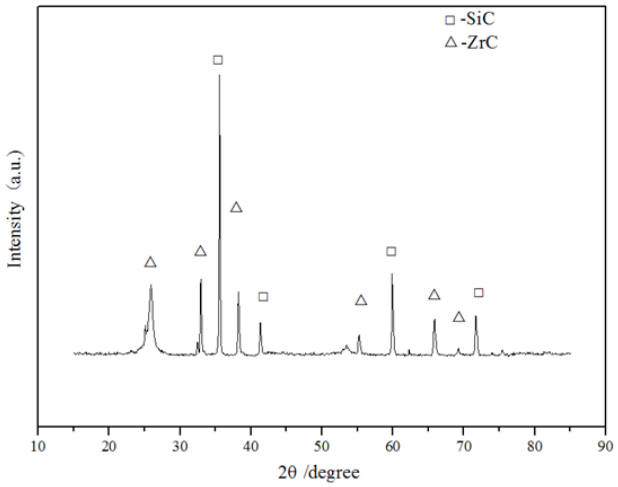

4 Impact of Si/Zr Mass Ratio in Infiltration Material on the Anti-ablation Performance of Composite Coatings

Table 2 presents the anti-ablation performance of C/C composite materials with Si-Zr-C composite coatings prepared with varying Si/Zr mass ratios in the infiltration material. It can be observed from the table that, after plasma ablation for 120 seconds, using mass ablation rate as the standard, the mass ablation rate first increases and then decreases with the increase in the Si/Zr mass ratio. The optimal anti-ablation performance is achieved when the Si/Zr mass ratio is 6:4, with a mass ablation rate of $-3.083\times10^{-5}g\cdot s^{-1}$. Sample 1 exhibits the poorest

anti-ablation performance, with a mass ablation rate of $1.259\times10^{-3}g\cdot s^{-1}$.

Table.2 Ablation properties of Si-Zr-C multilayer coating produced by different mass ratio of Si/Zr

No.	Si/Zr ratio	Mass before ablation/g	Mass after ablation/g	Time/s	Mass ablation rate/ / $g\cdot s^{-1}$
1	4:6	18.4316	18.2805	120	1.259×10^{-3}
2	5:5	17.9851	17.9709	120	1.183×10^{-4}
3	6:4	17.5651	17.5688	120	-3.083×10^{-5}
4	7:3	12.4646	12.4379	120	2.225×10^{-4}

Figure 16 shows the surface backscattered image of the ablation center of sample 3 after 120 seconds of plasma ablation at 2300℃. From the image, it can be observed that the coating surface remains smooth and dense after ablation, with no exposed substrate. The surface consists of two phases, gray and white, exhibiting a glassy appearance. Figure 17(a) and (b) respectively represent the energy spectrum analysis images at points 1 and 2 in Figure 16. Combined with the XRD analysis results in Figure 15, it can be inferred that the white phase is a mixture of $ZrSiO_4$, SiO_2, and ZrO_2, while the gray phase is SiO_2. The grains on the coating surface are large SiC particles that have not completely oxidized.

During the ablation process, the $ZrSi_2$ and SiC on the coating surface react with oxygen to generate SiO_2 and ZrO_2 respectively. SiO_2 and ZrO_2 further react to form $ZrSiO_4$. Since $ZrSi_2$ and SiC exist separately on the coating surface, a mixture of $ZrSiO_4$, SiO_2, and ZrO_2 is only formed in the vicinity of the $ZrSi_2$ phase. The SiC phase oxidizes to SiO_2, leaving a small amount of unoxidized SiC particles. Due to the ablation center temperature reaching 2300℃, higher than the melting point of SiO_2, SiO_2 exhibits a molten state and experiences significant loss under the action of high-speed gas flow. The formation of ZrO_2 and $ZrSiO_4$ enhances the stability of SiO_2 and provides good anti-ablation properties with low oxygen diffusion rate. Molten SiO_2 can flow and fill surface cracks, contributing to the overall excellent anti-ablation performance of the $ZrSi_2$-SiC-Si composite coating under the combined action of SiO_2 and the mixture of $ZrSiO_4$, SiO_2, and ZrO_2.

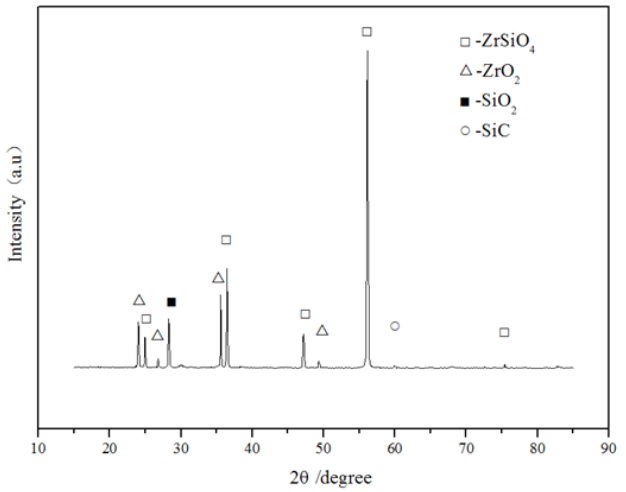

Figure 15 XRD patterns of sample 3 coating surface after ablation

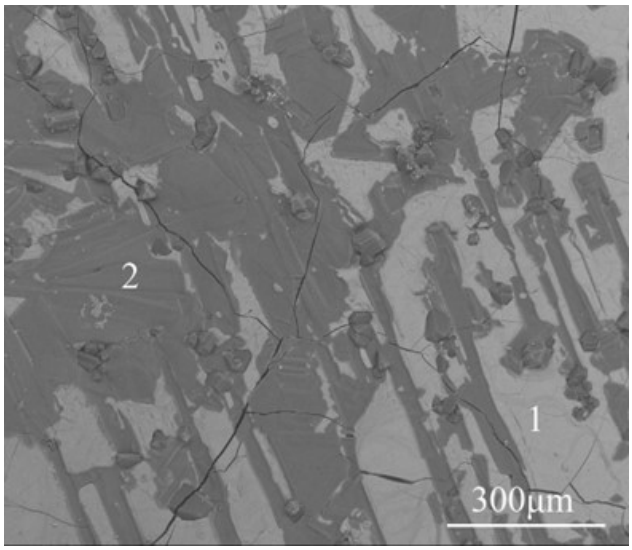

Figure 16 BSE image of ablation center in coating surface of sample 3 after ablation

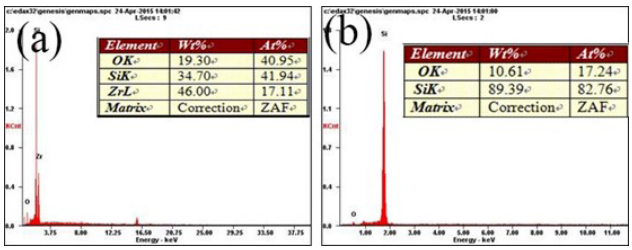

Figure 17 EDS analysis(a,b) of point 1,2 in surface of sample 3 coating

Due to the reactions of $ZrSi_2$ and SiC on the coating surface with oxygen to produce SiO_2 and ZrO_2, which are weight-increasing reactions, and the extremely low rate of oxygen diffusion through the coating to react with the substrate, the coating exhibits a weight gain overall. Therefore, the coating demonstrates excellent anti-ablation properties.

Figure18(a), (c), (e) and (b), (d), (f) respectively show the morphology of the ablation center and edge of samples 1, 2, and 4. From Figure 18, it can be observed that the substrate is exposed at the ablation center of sample 1, and the interfaces between carbon fibers/matrix and matrix/coating are prone to oxidation. The carbon fibers become needle-shaped after ablation. At the ablation edge, a loose layer of oxide is observed on the coating surface. During ablation, the coating experiences significant thermal stress and gas flow shear forces. Due to the large difference in thermal expansion coefficients between the ZrC coating and the SiC inner layer, the coating develops cracks under thermal stress. High-speed gas flow may cause the detachment of the coating. ZrC oxidation on the coating surface produces ZrO_2, which exists in granular form due to its high melting point compared to the ablation center temperature. Weak adhesion between ZrO_2 and the substrate causes it to be blown away by the high-speed gas flow, exposing the SiC inner layer. Additionally, molten SiO_2 produced by the SiC inner layer under gas flow is easily carried away from the substrate. Consequently, the coating loses its protective function, and the exposed substrate undergoes oxidation. In the ablation edge area, where the gas flow velocity is lower, some loose ZrO_2 particles remain on the coating surface.

In Figure 18(c) and (d), it is observed that the substrate is exposed and oxidized at the ablation center of sample 2, while a complete layer of oxide covers the ablation edge area. The ZrSi and SiC grains on the coating surface of sample 2 are large, and the grain boundaries are prominent. The significant presence of ZrSi, along with the substantial difference in thermal expansion coefficients between ZrSi and the SiC inner layer, leads to the generation of numerous cracks during both the preparation and ablation processes. Under thermal stress during ablation, surface cracks increase, and grain boundaries become regions for crack propagation. Consequently, under the action of high-speed gas flow, parts of the coating detach from the surface, exposing the substrate underneath, which is then ablated by the gas flow.

In Figure 18(e) and (f), it can be observed that the substrate is exposed and oxidized at the ablation center, while the oxide product is loose at the ablation edge of sample 4. Sample 4 has a lower content of ZrC phase, which cannot effectively improve the anti-ablation performance of the SiC coating. Therefore, the substrate at the ablation center undergoes oxidation.

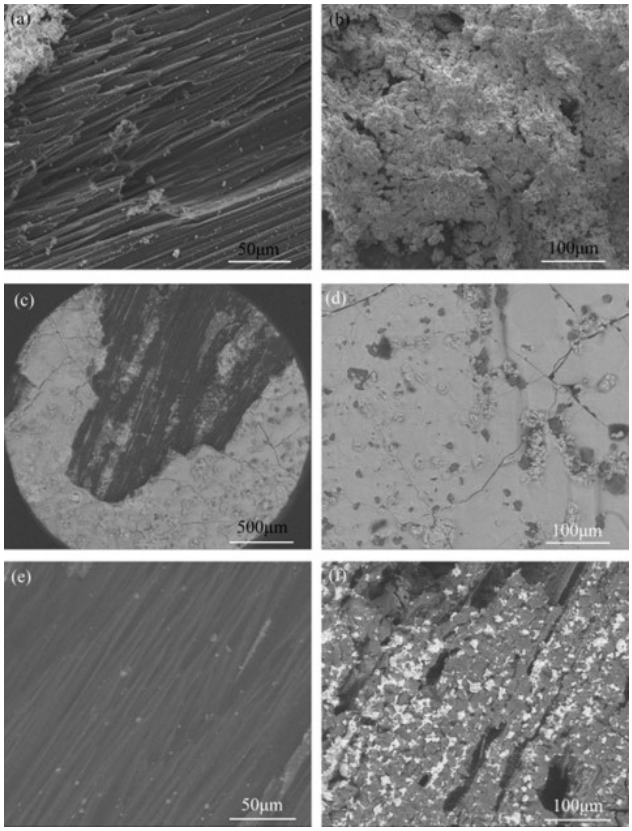

Figure 18 Surface micrographa of ablation center and edge of sample 1,2,4

5 Study on the Ablation Mechanism of Zr-Si-C Composite Coating on C/C Composite Material

The ablation of materials is a complex process influenced by various factors, involving the combined effects of thermochemistry, thermophysics, and mechanical erosion.

5.1 Thermochemical Ablation Mechanism

During the ablation process, the following reactions may occur:

$ZrC(s)+O_2(g)=ZrO_2(s)+COn(g)$

$SiC(s)+O_2(g)=SiO_2(l)+ COn (g)$

$C(s)+O_2(g)=COn(g)$

$ZrO_2(s)+SiO_2(l)=ZrSiO_4(s)$

$ZrSi_2(s)+3O_2(g)=ZrO_2(s)+2SiO_2(l)$

$ZrSi(s)+2O_2(g)=ZrO_2(s)+SiO_2(l)$

$SiO_2(l)=SiO_2(g)$

5.2 Thermophysical Ablation Mechanism

Thermophysical ablation primarily refers to the melting and sublimation of the coating and reaction products. At the ablation temperature in this experiment, the melting point of SiO_2 produced by the coating reaction is below the ablation temperature, resulting in a molten state. Subsequent sublimation and volatilization of SiO_2 cause mass loss but also carry away heat from the ablation region, reducing the surface temperature of the coating.

5.3 Mechanical Erosion Mechanism

During ablation, the coating is subjected to the impact of high-speed, high-temperature, and high-pressure gas flow. Under high temperature, thermal stress on the coating surface generates cracks, leading to partial detachment under high-speed gas flow. The SiO_2 generated by oxidation on the coating surface is in a molten state at the ablation temperature, exhibiting low viscosity, which results in its disappearance due to gas flow erosion. Additionally, Reaction (7) causes partial volatilization of SiO_2, carrying away heat from the coating surface. ZrO_2 formed by oxidation on the coating surface has not reached its melting point and exhibits low adhesion to the substrate, making it susceptible to removal by high-speed gas flow. However, ZrO_2, along with the $ZrSiO_4$ produced by the reaction of SiO_2 and ZrO_2, enhances the stability of SiO_2 and exhibits good resistance to ablation, as well as a low oxygen diffusion rate, thereby improving the ablation resistance of the coating.

6 Conclusion

This chapter investigates the effect of the Si/Zr mass ratio in the embedding material on the structure, morphology, and ablation resistance of Zr-Si-C composite coatings on C/C composite materials.

(1) With the increase of Si/Zr mass ratio in the embedding material, the coatings obtained are as follows: SiC inner layer, ZrC outer layer of SiC-ZrC composite coating; SiC inner layer, SiC-ZrSi mixed outer layer of SiC-SiC-ZrSi composite coating; SiC inner layer, SiC-$ZrSi_2$ mixed outer layer of SiC-SiC-$ZrSi_2$ composite coating; SiC inner layer, SiC-ZrC mixed outer layer of SiC-ZrC composite coating. The SiC-ZrC composite coating has larger SiC grains in the outer ZrC layer, with pores between the grains. The ZrC content is relatively low and distributed discretely among the SiC grains.

(2) With the increase of Si/Zr mass ratio in the embedding material, the ablation resistance of the coatings first increases and then decreases. When the Si/Zr mass ratio is 6:4, the coating exhibits the best ablation resistance. After 120s of ablation, the mass ablation rate of the specimen is -3.083×10^{-5} $g \cdot s^{-1}$, with fewer cracks and grain boundaries on the coating surface, resulting in higher coating strength and less crack generation under thermal stress. Additionally, the reaction products ZrO_2 and $ZrSiO_4$ enhance the high-temperature stability of SiO_2, and they themselves exhibit good resistance to ablation as well as a low oxygen diffusion rate, thereby improving the ablation resistance of the coating. However, when the coating structure is SiC-ZrC with SiC as the inner layer and ZrC as the outer layer, thermal stress is generated in the coating due to the large difference in thermal expansion coefficients between the inner and outer layers, leading to crack formation and coating detachment during ablation. The ZrC oxidation product ZrO_2 cannot melt at the ablation temperature and exhibits weak adhesion to the substrate, making it easily removed by high-speed gas flow, thereby exposing the SiC inner layer and substrate, which is detrimental to the ablation resistance of the specimen.

Reference

[1] Song M.S., Huang B., Zhang M.X., et al. Formation and growth mechanism of ZrC hexagonal platelets synthesized by self-propagating reaction[J]. Journal of Crystal Growth, 2008, 310(18): 4290-4294.

[2] Craciun V., Craciun D., Howard J.M., et al. Pulsed laser deposition of crystalline ZrC thin films[J]. Thin Solid Films, 2007, 515(11): 4636-4639.

[3] Ozaki Y., Zee R.H., Investigation of thermal and hydrogen effects on emissivity of refractory metals and carbides[J]. Materials Science & Engineering A, 1995, 202(1-2): 134-141.

[4] Zhuang L., Fu Q.G., Li H.J., et al. Study on oxidation behavior and ablation resistance of C/C-ZrC-SiC composite materials prepared by polymer impregnation and pyrolysis method[J]. Materials Review, 2015, 34(6): 42431. (in Chinese)

[5] Liu S.X., Dong Z.J., Zhang X., et al. Effect of Si/Zr mass ratio on microstructure and oxidation resistance of SiC/ZrC coatings[J]. Surface Engineering, 2014, 27(3): 43-49. (in Chinese)

[6] Yang X., Huang Q.Z., Chang X., et al. Preparation of ZrC-SiC composite coating by graphite impregnation method with zircon sand[J]. Journal of Inorganic Materials, 2010, 25(1): 41-46. (in Chinese)

[7] Wang Y., Zhu X., Zhang L., et al. C/C–SiC–ZrC composites fabricated by reactive melt infiltration with Si0.87Zr0.13 alloy[J]. Ceramics International, 2012, 38(5): 4337-4343.

[8] Hu M.H., Li K.Z., Li H.J., et al. Double layer ZrSi2–ZrC–SiC/SiC oxidation protective coating for carbon/carbon composites[J]. Surface Engineering, 2015, 31: 33341.